Journal of Electronic Materials (2024) 53:5073–5082
https://doi.org/10.1007/s11664-024-11143-4

28TH INTERNATIONAL CONFERENCE ON NUCLEAR TRACKS AND RADIATION MEASUREMENTS

Modification of the Properties of CdSe Nanowires by Argon Ion Implantation

Chetna Narula[1] · R. P. Chauhan[2] · Ajay Garg[1] · Pallavi Rana[2] · Suresh Panchal[2] · Renu Gupta[3]

Received: 22 January 2024 / Accepted: 23 April 2024 / Published online: 21 May 2024

Abstract
Cadmium selenide (CdSe) represents a direct-bandgap semiconductor belonging to the II–VI group, operating within the visible range of the electromagnetic spectrum. Nanowires composed of CdSe hold significant potential for various optoelectronic applications. Employing ion implantation is an immensely appealing technique, which allows for a controlled introduction of dopants into any lattice, and it is based on well-established principles. In this context, the current investigation focuses on the impact of argon ion implantation on cadmium selenide nanowires with a diameter of 80 nm. The nanowires were synthesized via a template-assisted electrodeposition method using polycarbonate membranes with 80 nm pores and 10 µm thickness. A three-electrode setup facilitated their fabrication. Subsequently, argon ions with a 4+ charge state and an energy of 1 MeV were implanted into the synthesized nanowires at varying fluence levels, ranging from 10^{11} to 10^{13} ions/cm^2. The ion implantation process was conducted in the radiation chamber of the Inter-University Accelerator Centre's low-energy ion implantation facility in New Delhi, India. Stopping and Range of Ions in Matter (SRIM) code simulations were employed to determine the optimal implantation parameters. Compositional analysis confirmed the successful incorporation of argon ions into the CdSe lattice. Notably, scanning electron microscopy revealed no alterations in the nanowire morphology despite the implantation. X-ray diffraction analysis showed no shift in the 2θ position of diffraction peaks, but indicated variations in their intensities. Furthermore, the implanted nanowires exhibited an increased absorbance and improved conductivity with increasing ion fluence. These findings demonstrate the effectiveness of argon ion implantation in modifying the optical and electrical properties of 80 nm diameter CdSe nanowires.

Keywords Template synthesis · CdSe nanowires · argon ion implantation · optical properties · electrical properties

Introduction

In the twenty-first century, the key position of nanoscience/nanotechnology has been firmly established as its impact is recognized across a wide spectrum of disciplines. Investigation of nanomaterials and nanostructures to identify their usefulness is a key aspect of nanotechnology. One-dimensional semiconducting nanostructures, including nanowires, nanorods, nanobelts, nanotubes, and nanoribbons, have garnered extensive attention due to their unique size-dependent optical, electrical, and magnetic properties. These characteristics hold promise for diverse applications in optoelectronics, nanoscale electronics, sensors, and photovoltaics.[1,2]

Their exceptional properties stem from two key factors: a high surface-to-volume ratio and the confinement of photons and carriers within two dimensions. These remarkable features make them ideal building blocks for complex devices with vital applications. To fully realize these applications, precise control over crucial parameters like size, composition, crystal structure, and morphology is essential. This control ultimately determines the optical and electrical properties, paving the way for functional nanoscale devices.[3] During the most recent decade, significant efforts have been

✉ Chetna Narula
chetnanarula@gmail.com

R. P. Chauhan
chauhanrpc@gmail.com

[1] I.B. (PG) College, Panipat, Haryana, India

[2] National Institute of Technology, Kurukshetra, Kurukshetra, Haryana 136119, India

[3] S.D. (PG) College, Panipat, Haryana, India

devoted to the fabrication and exploration of nanoscale wide-bandgap II-VI group semiconductors because of their indispensable optoelectronic applications for optical devices.[4,5] Cadmium selenide (CdSe) one-dimensional nanostructures have enhanced effective photon absorption and a higher rate of electron transfer due to their attractive properties in the scattering of light, consequently increasing the proficiency of solar cells. To completely comprehend the conduct of these devices, it is vital to assimilate the optical and electronic properties of their building elements, that is, CdSe nanowires.

Ion implantation is a widely employed technique for manipulating the electrical, structural, and optical properties of various nanostructures. It offers several advantages over chemical methods, such as simpler processing, precise control over film stoichiometry, and environmental friendliness. These benefits make it a popular choice for the fabrication as well as manipulation of semiconductor nanostructure and devices. In ion implantation, impurity ions are deliberately injected into the target material to achieve the desired tuning. This technique is particularly effective for modifying the properties of nanostructured materials relative to their bulk counterparts. This enhanced impact stems primarily from the high surface area-to-volume ratio of nanomaterials, which amplifies the interaction between the implanted ions and the material.[6–8]

Ion beam technology is a fundamental tool in nanofabrication, driving the development of advanced electronic devices such as miniaturized transistors and highly efficient solar cells. By precisely sputter-etching nanostructures and introducing controlled dopants through ion collisions, engineers can fine-tune the electrical and optical properties of materials, leading to breakthroughs in device performance and functionality. While both surface sputtering and doping play critical roles, doping through ion implantation has garnered significant attention for its ability to precisely introduce specific impurities into specific locations within a material. This allows for targeted manipulation of electrical conductivity and bandgap engineering, paving the way for next-generation optoelectronic devices.[9]

Rodrigues et al. presented a comprehensive spectroscopic investigation of europium implantation and annealing in GaN thin layers and nanowires by employing photoluminescence (PL) excitation at room temperature, temperature-based steady-state PL and time-resolved PL.[10] Singh et al. demonstrated the fabrication of tandem p–n junctions in nanorods of ZnO with ion implantation of positive oxygen ions having energies of 50 keV and 350 keV. The morphology of the as-implanted and annealed samples was characterized based on atomic force microscopy (AFM), photoluminescence (PL) spectra, and current–voltage characteristics.[11] Khatter and Chauhan reported optical modifications in CdS nanorod mesh after implantation with 180 keV argon ions, where the optical bandgap was found to decrease.[12] Ikram-l-haq et al. reported the influence of implanted copper ions on ZnO films deposited on indium-tin-oxide-coated polyethylene terephthalate flexible plastic substrates. The bandgap energy of ZnO films was found to decrease and films showed enhanced photovoltaic performance.[13] Singh et al. reported the effect of 600 keV carbon ions on the structural and magnetic properties of ZnO thin films and revealed that the strain decreases post irradiation.[14] Research on the application of ion beam technology for modifying and fabricating nanostructured materials is still evolving and has many more avenues to explore.[3,15]

With this view, in the present study, template-assisted electrodeposition was employed for fabricating CdSe nanowires and the impact of implanting different doses of argon ions was investigated using advanced characterization techniques like scanning electron microscopy (SEM), x-ray diffraction (XRD), and ultraviolet–visible (UV–Vis) spectroscopy. The results of the study revealed a significant decrease in the optical bandgap and enhanced conductivity in the implanted nanowires, suggesting potential applications in efficient light-emitting devices

Experimental

Synthesis and Characterization

CdSe nanowires were synthesized via a template-assisted electrochemical deposition method. A unique feature of this approach involves the use of a three-electrode setup (Cu substrate as working electrode, platinum (Pt) wire as counter electrode, and silver/silver chloride (Ag/AgCl) as reference electrode). Chronoamperometry at −1 V is employed to achieve precise control over nanowire growth within 80 nm pores of polycarbonate membranes (using a BioLogic SP-240 potentiostat). Prior to deposition, a thin gold layer was sputtered onto the polycarbonate membrane (purchased from Whatman) for enhanced electrical contact. Characterization of the nanowires employed a diverse suite of techniques: JEOL JSM-6390LV SEM for detailed morphology analysis, Rigaku MiniFlex II x-ray diffractometer (XRD) for structural insights, UV–Vis spectroscopy for optical properties, and probe station measurements with a Keithley source meter for electrical characterization. Additionally, SRIM simulations aided in optimizing the 1 MeV argon ion implantation process.

Implantation Parameters

CdSe nanowire samples were positioned in the low-energy ion implantation facility at the Inter-University Accelerator Centre (IUAC), New Delhi. Precisely controlled

doses of 1 MeV Ar^{+4} ions (current fixed at 25 pnA) were scanned across a 1-cm^2 area on the nanowires, ensuring that implantation depths remained within the length of the nanowire (estimated at 10 µm using SRIM simulations).[16] The recorded particle fluence rates were 5×10^{11}, 1×10^{12}, 5×10^{12}, and 1×10^{13} ions/cm^2, allowing the analysis of the influence of varying implantation levels. Additionally, the electronic and nuclear stopping powers were evaluated to provide further insights into the implantation process and to optimize future experiments for tailoring the properties of the nanowires.

Results and Discussion

SRIM-TRIM Simulation

To understand the impact of argon ion implantation on the CdSe nanowires, Stopping Range of Ions in Matter (SRIM) 2013 (Ion Distribution with Quick Calculation of Damage) with the Kinchin–Pease formalism was employed, which accurately models the collision–cascade phenomenon and subsequent damage created by energetic ions. The simulations revealed a mean projected range of 0.726 µm for 1 MeV Ar^{+4} ions in CdSe, which is significantly smaller than the 10 µm nanowire length. Notably, both electronic and nuclear stopping powers ($dE/dx_{electronic}=9.867E+02$ k eV/micron, and $dE/dx_{nuclear}=2.232E+02$ keV/micron) contribute almost equally to the energy loss of the implanted ions, influencing their final distribution and potential for modifying the nanowire properties. Figure 1 visually depicts the implantation profile, where various colours represent implanted ions, displaced atoms (moving Cd and Se), and those brought to rest. Table I further details the energy loss breakdown, with categories like ionization, phonons, and target damage revealing insights into the mechanisms of energy transfer and potential alterations within the nanowires.

Analysis of Table I reveals that a significant portion of the incident energy is dissipated through ionization, primarily by both the implanted ions and recoiled target atoms. Energy loss to phonons exceeds that for target damage, likely due to the efficient conversion of kinetic energy from fast-moving ions into heat vibrations. This phonon generation might have played a role in modifying the electrical or optical properties of nanowires through lattice distortions. Figure 2 showcases the spatial distribution of displacements induced by the implanted argon ions. The plot clearly shows the localized nature of these displacements, with higher-density regions potentially coinciding with areas of high ionization loss as identified in Table I. While replacement collisions would not occur in this case due to the different material compositions, analysing the total number of generated displacements, vacancies, and recoil events provides valuable insights into the potential defect landscape created within

Table I SRIM-TRIM simulation results for % energy loss

% Energy loss	Ions	Recoils
Ionization	62.92	9.47
Vacancies	0.06	1.25
Phonons	0.22	26.08

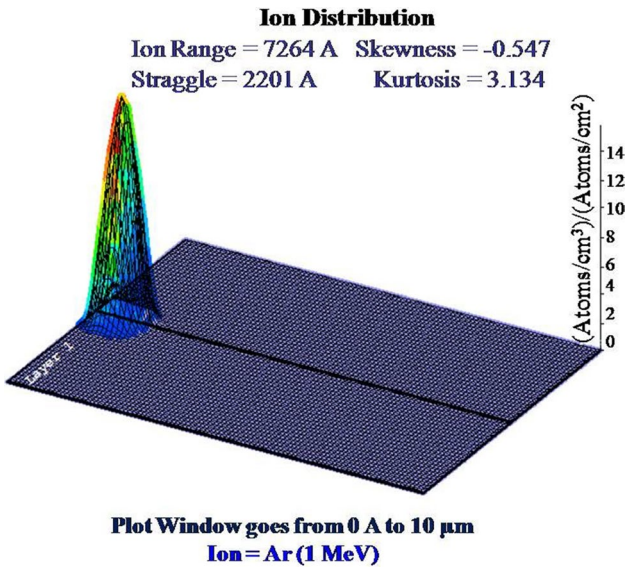

Fig. 1 SRIM simulation for distribution of implanted 1 MeV argon ions in CdSe target.

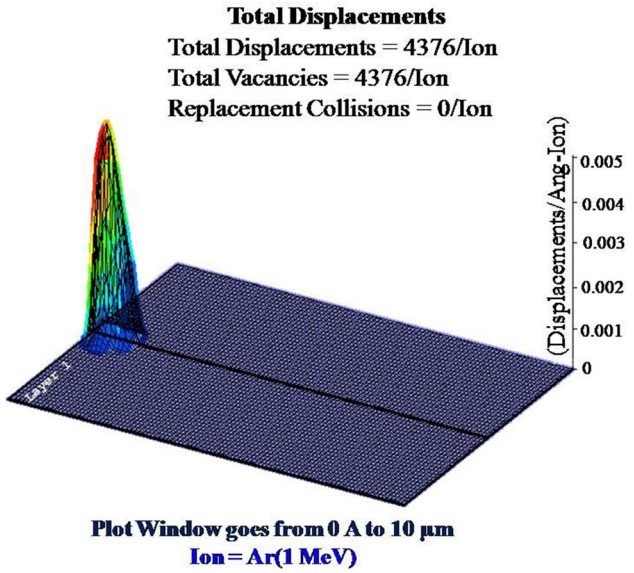

Fig. 2 Spatial distribution of displacements caused by 1 MeV argon ions in CdSe target.

the nanowires by the implantation process. It is important to note that SRIM simulations focus solely on collision dynamics and do not account for thermal effects like annealing, which might influence the final defect configuration.

Morphological and Elemental Study

Figure 3a depicts the typical morphology of CdSe nanowires fabricated within the template. As expected, the nanowires exhibit a uniform diameter of approximately 80 nm and lengths reaching around 10 µm, mirroring the pore dimensions of the template used for their growth. However, some nanowires appear shorter, possibly due to breakage during the template dissolution process. Figure 3b presents SEM images of the nanowires after argon ion implantation. Notably, no discernible changes in morphology or deformation are observed in the ion-bombarded samples compared with the pristine ones.

Chemical composition analysis of pristine and argon ion-implanted CdSe nanowires was performed using energy-dispersive x-ray spectroscopy (EDS), as shown in Fig. 4. The EDS spectrum in Fig. 4a exhibits characteristic peaks for Cd and Se, with an approximate intensity ratio of 1:1, indicative of stoichiometric CdSe formation. The presence of unidentified peaks is attributed to the underlying copper substrate and is disregarded in the composition analysis. As expected, the implanted nanowires (Fig. 4b) exhibit an additional peak corresponding to the characteristic x-ray emission of implanted argon ions, confirming their successful incorporation into the CdSe nanowire structure.

Structural Study

This study investigates the impact of argon ion implantation on the structural parameters of CdSe nanowires of 80 nm diameter. High-resolution electron microscopy reveals minimal morphological changes following implantation, indicating a robust structural response to ion bombardment. However, x-ray diffraction analysis suggests subtle alterations in the crystal lattice order, potentially influencing the nanowire properties. X-ray diffraction (XRD) analysis, employing CuKα radiation ($\lambda = 1.5406$ Å), was performed on both pristine and argon ion-implanted CdSe nanowires to investigate their crystal structure and phase (Fig. 5a and b). Measurements were recorded within the 2θ range of 20°–100° with a step size of 0.02°. Comparison of the diffraction peaks with the CdSe JCPDS card (77-2307) confirmed the presence of the expected hexagonal wurtzite CdSe phase in all samples. Prominent peaks were identified at 2θ values of 25.3°, 41.9°, 45.8°, 74.3°, 76.7°, 82.4°, and 89.2°, corresponding to the (002), (110), (103), (204), (300), (302), and (214) planes, respectively. The XRD patterns revealed no significant shifts or broadening of the diffraction peaks in the implanted nanowires (Fig. 5) compared with the pristine samples (Fig. 5), suggesting minimal alterations in the overall crystal structure upon argon ion doping. Additionally, the absence of any extra peaks further corroborates the preservation of the CdSe phase. The presence of multiple well-defined peaks also confirms the polycrystalline nature of the nanowires. However, variation in the intensities of the peaks was observed after implantation. The intensity of the (002) peak in the implanted samples (Fig. 5) was observed to increase significantly compared with the other planes. This implies that the ion bombardment preferentially affects the orientation of the CdSe lattice along the c-axis, potentially inducing modifications in the crystallite texture or preferred growth direction of the nanowires.

Peak intensity changes in XRD spectra of implanted nanowires might be linked to crystallite size and lattice defects. While implantation creates defects, its dominant

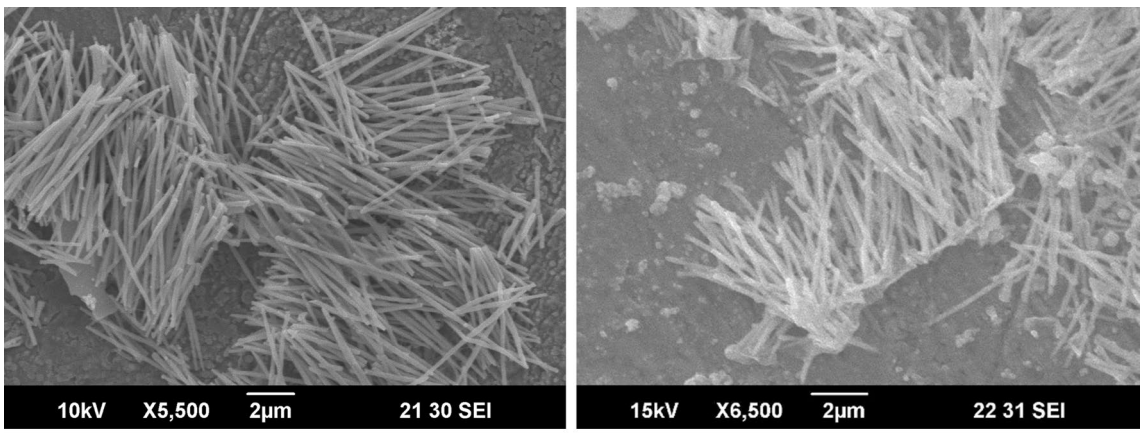

Fig. 3 SEM micrographs for (a) pristine 80 nm CdSe NWs and (b) argon ion-implanted CdSe NWs at a fluence of 1×10^{13} ions/cm^2.

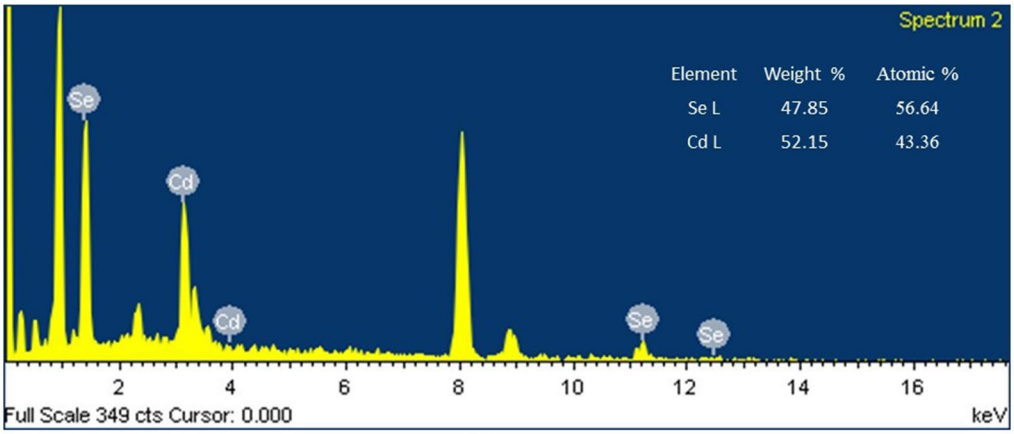

(a)

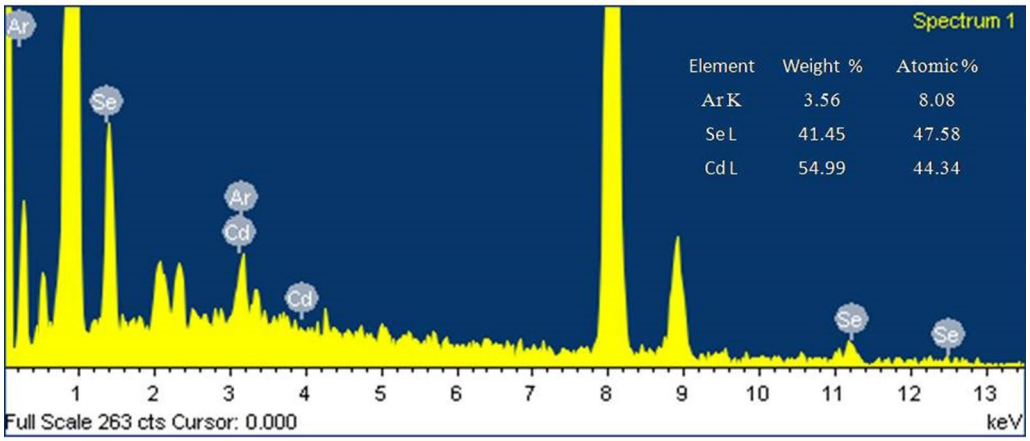

(b)

Fig. 4 (a) EDS spectrum of pristine CdSe nanowires, (b) EDS spectrum of argon ion-implanted CdSe nanowires at a fluence of 1×10^{13} ions/cm^2.

nuclear energy loss mechanism also influences plane orientation, contributing to observed intensity variations.

It is important to acknowledge that ion bombardment inevitably induces lattice disorder, with the extent of irregularity directly influenced by both ion energy and mass. In extreme cases, specific conditions can even lead to complete amorphization of the material. However, in our research, we achieved the controlled formation of polycrystalline CdSe nanowires with a preferential crystallite orientation through argon ion implantation. To quantify the observed preferential crystallite orientation within the CdSe nanowires, a comprehensive texture analysis was employed. As detailed in our previous works,[17,18] this method utilizes texture coefficients to numerically capture the relative intensity distribution of specific crystallographic planes. Accordingly, the texture coefficients for both pristine and argon ion-implanted nanowires were calculated, with the results summarized in Table II.

Computational TRIM (Transport of Ions in Matter) simulations provided valuable insights into the energy deposition profile of implanted argon ions within the CdSe nanowires. A significant portion of the ion energy was transferred to phonons, inducing lattice vibrations. As the implantation fluence increased, the (002) plane emerged as the preferred orientation, as reflected in the XRD analysis. It is suggested that the lattice vibrations triggered by energy lost to phonons may have facilitated the preferential reorientation of crystal planes, causing the observed variations in peak intensity. Further, comprehensive characterization of crystallite size, strain, and dislocation density (δ) was conducted for both pristine and implanted samples, their values are summarized in Table III.

To accurately determine the crystallite size of the CdSe nanowires, the x-ray line broadening method based on the Scherrer equation[18] was employed. However, it is important to acknowledge that peak broadening in XRD spectra

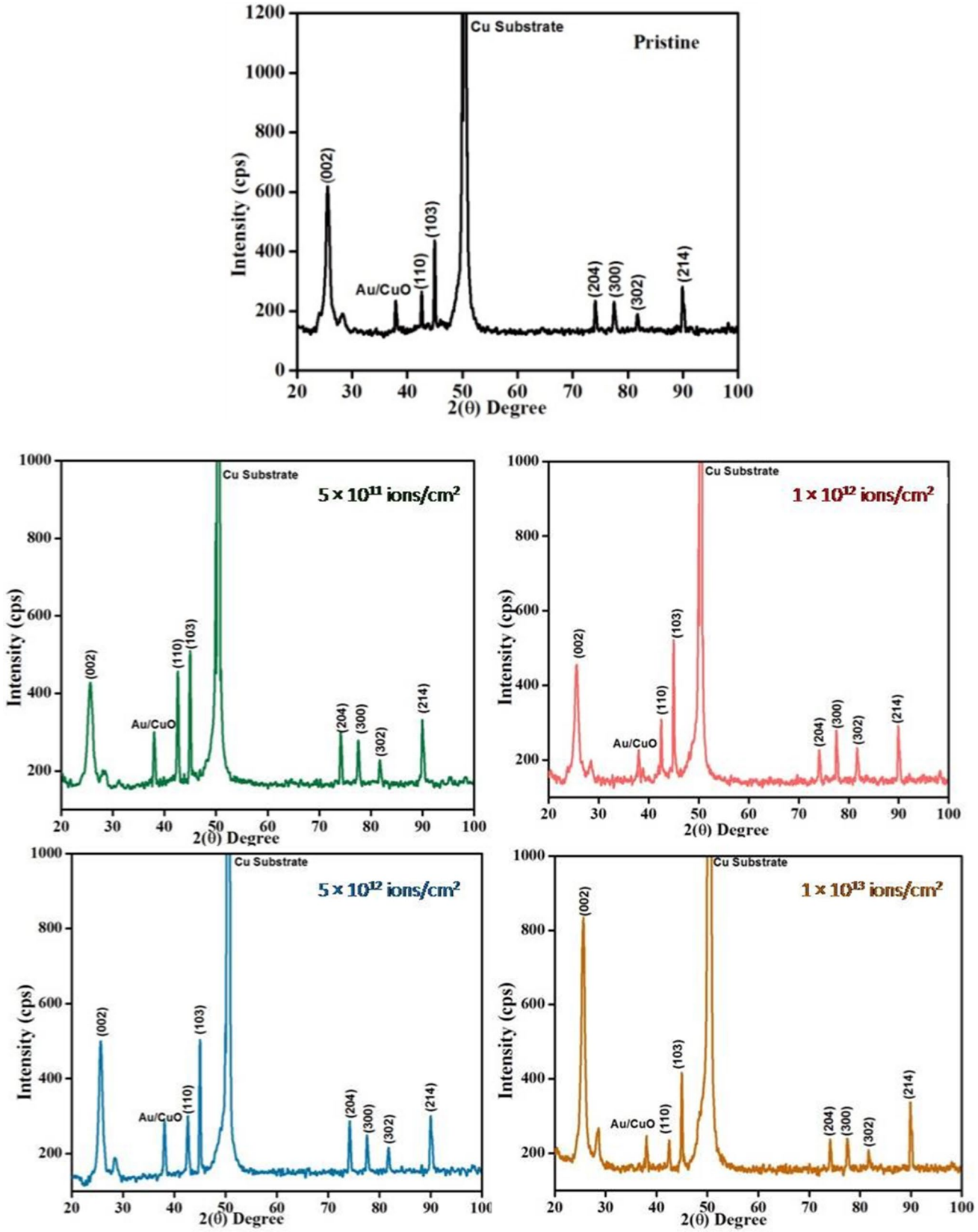

Fig. 5 XRD spectra of pristine and argon ion-implanted CdSe nanowires at various ion fluence levels, respectively.

Table II Texture coefficient analysis of argon ion implantation in CdSe NWs

Sr. no.	Plane, hkl	Texture coefficient at given ion fluence, ions/cm^2				
		0	5×10^{11}	1×10^{12}	5×10^{12}	1×10^{13}
1	002	*1.89 ± 0.07*	*1.06 ± 0.13*	*1.10 ± 0.06*	*1.46 ± 0.03*	*2.09 ± 0.07*
2	110	0.28 ± 0.09	0.66 ± 0.08	0.29 ± 0.12	0.33 ± 0.12	0.12 ± 0.17
3	103	0.55 ± 0.02	0.78 ± 0.07	0.72 ± 0.10	0.80 ± 0.09	0.43 ± 0.15
4	300	*1.26 ± 0.03*	*1.54 ± 0.11*	*1.76 ± 0.19*	*1.33 ± 0.13*	0.95 ± 0.08
5	302	*1.01 ± 0.23*	0.95 ± 0.15	*1.14 ± 0.16*	*1.06 ± 0.07*	0.51 ± 0.14

Preferred orientations, for which the value of texture coefficient (TC) is greater than 1 are mentioned in italics

Table III Crystallite size, lattice strain and dislocation density values for pristine and argon ion-implanted samples

Sample	Average crystallite size, nm	Lattice strain ($\times 10^{-3}$)	Dislocation density ($\times 10^{15}$), m^{-2}
Pristine	20.91	4.21	2.29
Ar^{+4} 5×10^{11} ions/cm^2	21.18	4.64	2.22
Ar^{+4} 1×10^{12} ions/cm^2	23.01	3.99	1.89
Ar^{+4} 5×10^{12} ions/cm^2	25.02	3.80	1.59
Ar^{+4} 1×10^{13} ions/cm^2	26.29	3.66	1.44

can arise from multiple factors beyond just crystallite size, including lattice structure and internal strain (ε) induced by non-uniform atomic displacements during nanowire preparation.[19]

To account for these additional contributions, the theoretical Stokes–Wilson formula

$$\varepsilon = \beta/4\tan\theta \quad (1)$$

was used to separate the lattice deformation (ε) from the overall peak broadening, with θ being the Bragg's angle and β the full width at half maximum (FWHM) of the peaks.[20] Finally, recognizing the potential imperfections in the crystal lattice due to grain boundaries, stacking faults, and dislocations, the dislocation density (δ) was further evaluated using the empirical Williamson–Smallman equation

$$\delta = 1/D^2 \quad (2)$$

As this equation indicates, δ is inversely proportional to the square of the crystallite size (D^2), meaning higher dislocation density implies smaller crystallites and the presence of significant defects within the samples.[21] Dislocations in crystals interact through their strain fields: the same Burger's vector leads to repulsion, where opposite attracts/annihilates. Most materials have dislocations from the start (stresses during formation). Ion implantation creates point defects (interstitials, vacancies) that can recombine and form extended defects during annealing. Different types of defects depend on the type of implant, implant dose, energy, and thermal energy generation. Despite the potential for damage, high-energy implantation in our study led to larger crystallites, lower dislocation density, and reduced strain. This suggests a unique behaviour where defect creation is overshadowed by defect annihilation processes, potentially triggered by the combined effects of ion bombardment and thermal annealing. This phenomenon opens exciting avenues for tailoring the nanowire microstructure and achieving optimal properties for various applications.[22–25]

Optical and Electrical Study

To further elucidate the electronic properties of the nanowires, UV–Vis absorption spectra were investigated and recorded within the wavelength range of 480–750 nm (Fig. 6a). The observed absorption edge lies at a significantly lower wavelength than the bulk CdSe value of 712 nm. This characteristic blue shift in light absorption is a well-known signature of size confinement effects in nanomaterials, indicating the influence of quantum confinement on the electronic band structure of the CdSe nanowires.

To quantitatively assess the electronic structure modifications induced by ion implantation, the optical bandgap (Eg) of the CdSe nanowires was determined using the well-established Tauc and Menth method.[26] This method relies on the relationship between the absorption coefficient (α), photon energy ($h\nu$), and Eg expressed as $(\alpha h\nu) = k(h\nu - Eg)^n$, where k is a constant and n depends on the type of electronic transition involved. In Fig. 6b, plots of $(\alpha h\nu)^2$ versus $h\nu$ are presented, with the intercept on the energy axis providing the direct measurement of Eg. Table IV summarizes the Eg values obtained from the Tauc plots for different implantation fluence rates.

The present study revealed a progressive decrease in the bandgap of the CdSe nanowires as the implantation fluence is increased. This observation can be attributed to a complex interplay of several factors including quantum size effects due to the confined geometry of the nanowires, randomization of grain distribution potentially altering energy

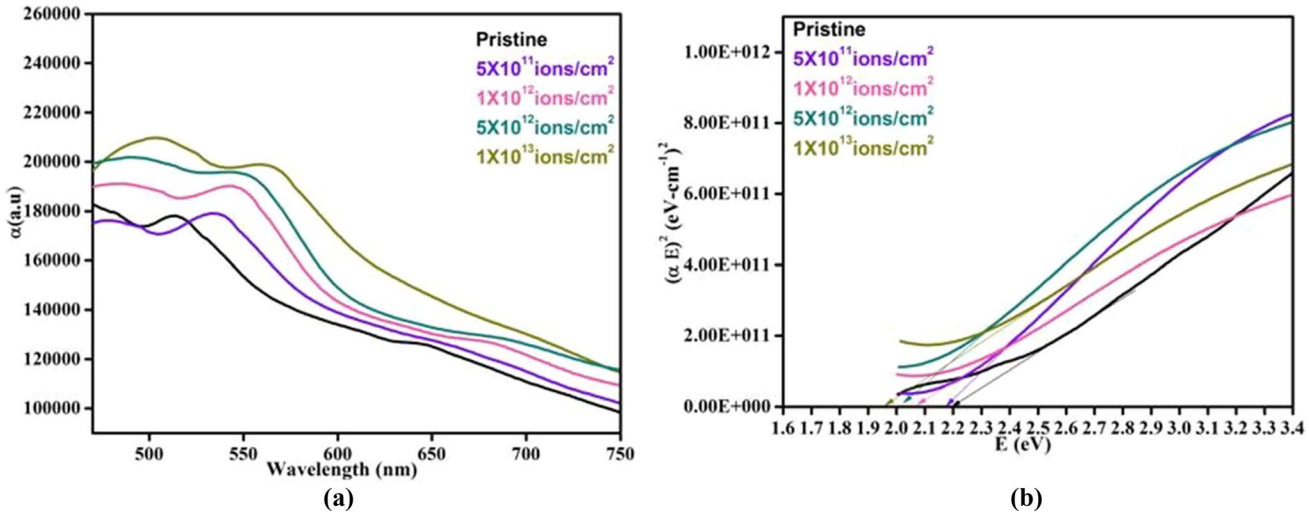

Fig. 6 (a) Plot of absorption coefficient (α) versus wavelength (λ) at different fluence rates of argon ion implantation and (b) Tauc plot for argon implantation.

Table IV Optical bandgap and electrical conductivity of pristine and argon ion-implanted CdSe nanowires at various fluence

Fluence, ions/cm^2	Optical bandgap, eV	Electrical conductivity, Ω^{-1} cm^{-1}
0	2.20	7.52
5×10^{11}	2.17	9.50
1×10^{12}	2.09	34.78
5×10^{12}	2.02	42.41
1×10^{13}	1.97	42.76

pathways, increased defect density impacting electronic states, and variations in crystallite size influencing electron confinement. The literature suggests that changes in grain size can directly influence the bandgap through alterations in confinement effects. Additionally, previous studies have demonstrated the ability of ion implantation to introduce lattice irregularities, potentially contributing to further modifications in the nanowire optical properties, likely due to the presence and varying levels of defects.[22]

Pre-dissolution *I–V* measurements were performed on ~ 470 vertically aligned CdSe nanowires of 80 nm diameter using a two-probe setup and a Keithley 2400 source measure unit. The observed linear *I–V* characteristics (Fig. 7), as captured by the first-order polynomial fitting, suggest that carrier transport within the CdSe nanowires falls within the diffusive regime.

This allows for the application of Ohm's law to describe the electrical behaviour. Consequently, we calculated the electrical conductivity (σ) using the following equation, where l represents the nanowire length, A denotes its cross-sectional area, and dI/dV is the slope of the *I–V* curve:

$$\sigma = (\mathrm{d}I/\mathrm{d}V) * (l/A) \tag{3}$$

The inverse of the slope in the *I–V* graphs provides a direct measure of the average resistance of the CdSe nanowires at each implantation fluence. By employing Eq. 3 and considering the dimensions of individual nanowires, the corresponding conductivity values were determined as summarized in Table IV. The symmetric and linear nature of the *I–V* curves within the measured voltage range (Fig. 7) further supports the validity of Ohm's law in this context. The polycarbonate (PC) membrane's conductivity (10^{-14} Ω^{-1} cm^{-1}) is insignificant relative to that of CdSe nanowires, ensuring our *I–V* measurements capture only the nanowire behaviour.[27]

Energetic ions traversing a solid lose energy through 'nuclear' and 'electronic' stopping. These interactions cause various excitations and ionizations, impacting material properties like electrical conductivity. Ionization-generated electrons influence electrical properties, but only if they avoid trapping at point defects.[28]

To gain insights into the nature and extent of defect formation upon argon ion implantation at 1 MeV, we employed the TRIM simulation code. The analysis revealed that a significant portion of the ion's energy is dissipated through damage creation within the target material. Electrons along the ion's path undergo frequent scattering and excitation, subsequently transferring substantial energy to the lattice via electron–phonon coupling, potentially inducing localized heating. When the deposited energy in both electronic and atomic structures becomes comparable, the overall material response hinges on the intricate interplay of electronic excitations, point defects, and structural rearrangements.[29,30]

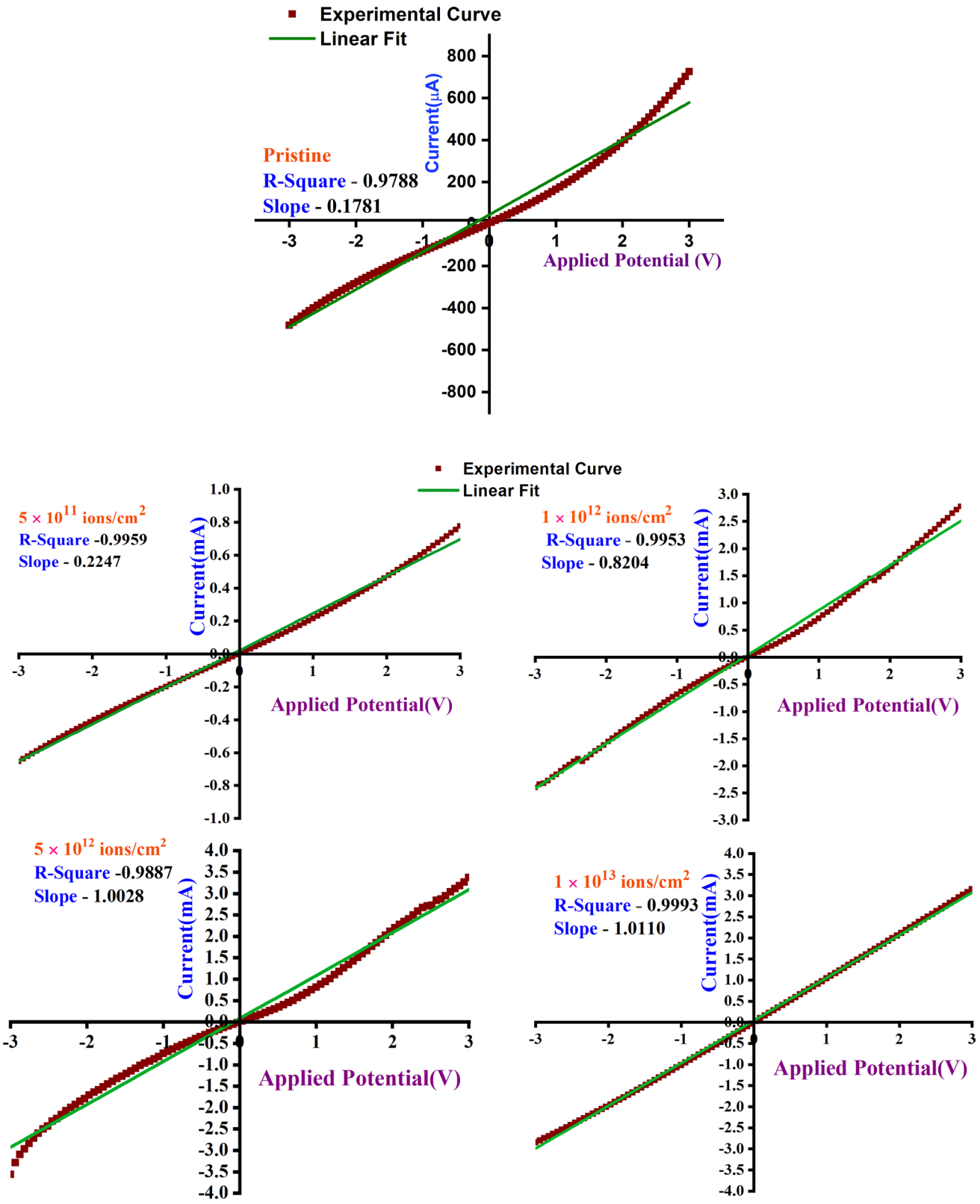

Fig. 7 *I–V* characteristics of pristine and argon ion-implanted 80 nm CdSe nanowires.

In argon-implanted CdSe nanowires, electrical conductivity improved with fluence which may be attributed to the produced ionization and reduced bandgap. The movement of the generated charge carriers on implantation and consequently the electrical conduction is enhanced. From structural analysis, it is observed that ion implantation influenced the grain size of the CdSe nanowires. This influence appears to follow a temperature-dependent trend, with implanted samples exhibiting both increases in average grain size and a reduction in the total number of grain boundaries. This phenomenon can be attributed to a defect-driven process known as dynamic annealing, where the energy deposited by the ions promotes the migration and reorganization of atoms, leading to grain growth and boundary coalescence.[31] The observed increase in grain size is further corroborated by the x-ray diffraction (XRD) analysis, which potentially contributes to the increased current observed in the implanted nanowires.

Conclusion

The present study demonstrates that argon ion implantation significantly impacts the optical and transport properties of CdSe nanowires. Remarkably, this manipulation occurs without any noticeable alterations in the diffraction peak positions, signifying minimal disruption to the underlying crystal structure. Implantation leads to an increase in charge carrier concentration, contributing to enhanced current flow and improved electrical characteristics. This observation highlights the potential of ion implantation as a powerful tool for modifying the functionality of semiconducting nanowires while maintaining their structural integrity.

Acknowledgments The authors wish to acknowledge the Director, IUAC, New Delhi, for providing the Low Energy Ion Beam Facility.

Conflict of interest The authors declare that they have no conflict of interest.

References

1. P.C. McIntyre and A. Fontcuberta i Morral, *Mater. Today Nano* 9, 100058 (2020).
2. N.P. Dasgupta, J. Sun, C. Liu, S. Brittman, S.C. Andrews, J. Lim, H. Gao, R. Yan, and P. Yang, *Adv. Mater.* 26, 2137 (2014).
3. C.Y. Hsu, A.M. Rheima, Z. Sabri Abbas, M.U. Faryad, M.M. Kadhim, U.S. Altimari, A.H. Dawood, A. Dhari Jawad Al-Bayati, Z.T. Abed, R.S. Radhi, A.S. Jaber, S.K. Hachim, F.K. Ali, Z.H. Mahmoud, G. Behzadi Pour, and E. Kianfar, *South African J. Chem. Eng.* 46, 286 (2023).
4. M. Nehra, N. Dilbaghi, G. Marrazza, A. Kaushik, R. Abolhassani, Y.K. Mishra, K.H. Kim, and S. Kumar, *Nano Energy* 76, 104991 (2020).
5. M.N. Yoder, *IEEE Trans. Electron Devices* 43, 1633 (1996).
6. M. Kaur, S. Gautam, and N. Goyal, *Mater. Lett.* 309, 131356 (2022).
7. A. Jafari, K. Tahani, D. Dastan, S. Asgary, Z. Shi, X.T. Yin, W.D. Zhou, H. Garmestani, and Ş Ţălu, *Surf. Interfaces* 18, 100463 (2020).
8. A. V. Krasheninnikov and K. Nordlund, *J. Appl. Phys.* **107**, (2010).
9. W. Li, X. Zhan, X. Song, S. Si, R. Chen, J. Liu, Z. Wang, J. He, and X. Xiao, *Small* 15, 1 (2019).
10. J. Rodrigues, M.F. Leitão, J.F.C. Carreira, N. Ben Sedrine, N.F. Santos, M. Felizardo, T. Auzelle, B. Daudin, E. Alves, A.J. Neves, M.R. Correia, F.M. Costa, K. Lorenz, and T. Monteiro, *J. Phys. Chem. C* 120, 6907 (2016).
11. A. Singh, K. Senapati, D.P. Datta, R. Singh, T. Som, S. Bhunia, D. Kanjilal, and P.K. Sahoo, *Nucl. Instrum. Methods Phys. Res., Sect. B* 409, 143 (2017).
12. J. Khatter and R.P. Chauhan, *Mater. Lett.* 307, 131082 (2022).
13. M.I. Khan, M. Irfan, M. Fatima, H.H. Somaily, Z.M. Elqahtani, and N. Alwadai, *Ceram. Int.* 49, 29622 (2023).
14. S. Singh, P. Poswal, B. Sundaravel, S. Chakravarty, and N. Shukla, *Mater. Chem. Phys.* 315, 129002 (2024).
15. L. Huang, H. Wu, G. Cai, S. Wu, D. Li, T. Jiang, B. Qiao, C. Jiang, and F. Ren, *ACS Nano* 18, 2578 (2024).
16. J.F. Ziegler, M.D. Ziegler, and J.P. Biersack, *Nucl. Instrum. Methods Phys. Res., Sect. B* 268, 1818 (2010).
17. C. Narula and R.P. Chauhan, *Radiat. Phys. Chem.* 144, 405 (2018).
18. B.D. Cullity, Elements of x-ray diffraction, Addison-Wesley Publishing(1956)
19. D. Dastan, S.L. Panahi, and N.B. Chaure, *J. Mater. Sci. Mater. Electron.* 27, 12291 (2016).
20. S.A.A. Terohid, S. Heidari, A. Jafari, and S. Asgary, *Appl. Phys. A Mater. Sci. Process.* 124, 1 (2018).
21. G.K. Williamson and R.E. Smallman, *Phil. Mag.* 1, 34 (1956).
22. D.C. Agarwal, D.K. Avasthi, F. Singh, D. Kabiraj, P.K. Kulariya, I. Sulania, J.C. Pivin, and R.S. Chauhan, *Surf. Coat. Technol.* 203, 2427 (2009).
23. A.J. Perry, J.R. Treglio, V. Valvoda, and D. Rafaja, *J. Vac. Sci. Technol. A Vac. Surf. Films* 13, 1067 (1995).
24. J. W. Mayer, In 1973 International Electron Devices Meeting, IEEE, 1973, pp. 3-5
25. D.E. Alexander and G.S. Was, *Phys. Rev. B* 47(6), 2983 (1993).
26. J. Tauc and A. Menth, *J. Non-Cryst. Solids* 8–10, 569 (1972).
27. R.M. Radwan, A.M. Abdul-kader, and A.E. Ali, *Nucl. Instrum. Methods Phys. Res. B: Beam Interact. Mater. At.* 266, 3588–3594 (2008). https://doi.org/10.1016/j.nimb.2008.06.011
28. J.F. Ziegler and J.P. Biersack, *Treatise on Heavy-Ion Science* (US, Boston, MA: Springer, 1985), pp.93–129.
29. C. Ronning, C. Borschel, S. Geburt, and R. Niepelt, *Mater. Sci. Eng. R. Rep.* 70, 30 (2010).
30. P. L. Degen, *Physica Status Solidi (A)*, 16 (1), 9–42 (1973).
31. Z.J. Wang, H. Kokawa, H. Takizawa, M. Ichiki, and R. Maeda, *Appl. Phys. Lett.* 86, 212903 (2005).